CFD simulation of multi-scale mixing in anionic polymerization tubular reactors

Le Xie, Li-Tao Zhu, Zheng-Hong Luo*
Department of Chemical Engineering, College of Chemistry and Chemical Engineering, Shanghai Jiao Tong University, Shanghai 200240, P. R. China
*Correspondence: Z.-H. Luo (E-mail: luozh@sjtu.edu.cn.edu.cn), Department of Chemical Engineering, College of Chemistry and Chemical Engineering, Shanghai Jiao Tong University, Shanghai 200240, P. R. China

Abstract

The molecular properties of polymers are greatly influenced by operation parameters during polymerization in reactors. Operation parameter distributions in reactors also result in molecular property distributions. Thus, polymerization bridges the gap between molecular properties and operation parameters. In the present study, coupling of CFD technology and method of moments to form a uniquely coupled model was used to describe multi-scale mixing fields in the reactor. The coupled model was validated using open experimental data and the effects of polymerization kinetics on macroscopic and microscopic fields were investigated numerically. Also, the coupled model was applied to predict the effects of some key operation conditions on the main macroscopic flow field parameters and polymer molecular proprieties numerically.
Keywords: Computational fluid dynamics, Kinetics, Modeling, Polymerization, Tubular reactor

1 Introduction

Tubular reactors have been widely applied in both laboratory and industry because of their simple and easy operation [1-5]. However, utilization of tubular reactors is still challenging [3, 6, 7]. In general, mixing has profound effects on reactor transfer performance and thereby restricts its scale-up [8, 9]. Therefore, describing the mixing behavior of the tubular reactor is necessary. Moreover, predicting the mixing behavior in such reactors is one of the challenges. By contrast, for the polymerization system that occurs in such tubular reactors, complexity of polymerization kinetics results in greater difficulty because polymerization kinetics involves various elementary reactions, rapid increase in viscosity, and uniqueness of polymerization system for heterogeneity and multiscale features [10-12]. Furthermore, polymerization is a strongly exothermic reaction. If the reaction heat is not removed in time, then the formed hot spots will further complicate reactor behavior, which may affect polymer properties [13].

For such polymerization systems, mixing shows multi-scale behaviors, i.e., macroscopic-scale and microscopic-scale [14-16]. On the one hand, macroscopic-scale mixing can be described

Received: October 25, 2015; revised: February 17, 2016; accepted: February 25, 2016

To be cited as: Chem. Eng. Technol. 10.1002/ceat.201500628

Link to final VoR: http://dx.doi.org/10.1002/ceat.201500628

via reactor operation parameter distributions (such as temperature, monomer concentration, and polymer concentration); on the other hand, microscopic-scale mixing can be investigated using polymer microscopic property profiles [such as number-average molecular weight (M_n) and dispersity index (PDI)] [9, 14, 15]. Polymer molecular properties can be greatly influenced by polymerization operation parameters. Improper macroscopic mixing leads to the uneven operation parameter distributions, which changes polymerization rate profiles in reactors and subsequently causes polymer microscopic property distributions [14-16]. Therefore, two scales of mixings are closely related via polymerization rate bridges. Indeed, the current study deals with three parameters, namely, operation condition – macroscopic-scale mixing – microscopic-scale mixing.

Currently, many reports dealt with mixing in reactors. Kolhapure and Fox [9] applied a multi-environment CFD micro-scale mixing model in describing small-scale mixing of chemical species in a tubular low-density polyethylene (LDPE) reactor under different operating conditions. In their CFD model, a comprehensive ethylene polymerization kinetic scheme was incorporated. Therefore, their model can predict the operation parameter and polymer microscopic property distributions. Unfortunately, a quasi-empirical Lagrangian micromixing model was added into the CFD model for micromixing behavior [17, 18]. The triplet "operation condition–macroscopic-scale mixing–microscopic-scale mixing" study was not pointed out [9]. Zhou et al. [16] simulated LDPE tubular and autoclave reactors using a CFD model coupled with polymerization reaction model. In their work, the method of moments was used to solve the polymerization reaction model. However, effects of operation parameters, such as temperature and monomer concentration, on multi-scale mixing behavior are disregarded, and only the simulated data at steady-state operation were recorded. Moreover, Meszéna and Johnson [14] also applied a CFD model that incorporates a polymerization kinetic scheme for predicting spatial distribution of the average molecular weights in living polymerization reactors at steady-state operation. However, only initiation and propagation steps were involved in their polymerization scheme. Recently, Roudsari et al. [10] developed a CFD model to study methyl methacrylate (MMA) solution polymerization in a lab-scale stationary continuous stirred tank reactor (CSTR) equipped with an impeller. A MMA polymerization kinetic model was also coupled into the CFD model. However, in their work, the selected reactor is a CSTR rather than tubular reactor, and multi-scale mixing was not involved. Inglès et al. [15] studied turbulent mixing in a polymerization reactor model experimentally and numerically. The model corresponds to a zone of an autoclave reactor installed with a stirrer. More recently, Zhu et al. [11, 12] in Luo's group developed a multi-scale product model to characterize polypropylene (PP) formation dynamics in catalytic FBR. Gas–solid flow field, morphological and molecular properties of particles, as well as their dynamics can be simultaneously obtained by solving the unique model that couples CFD model, population balance model, and moment equations. However, in their work, the selected reactor is also not a tubular reactor, and multi-scale mixing was not included in the study of Luo et al. In summary, the abovementioned investigations can be categorized as efforts of single-scale mixing modeling under steady-state operation rather than multi-scale mixing modeling in polymerization tubular reactors.

The current study aims to develop a new model that couples CFD technology and method of moments that can predict multi-scale mixing behavior in polymerization tubular reactors, and thus achieve a triplet "operation condition–macroscale mixing–microscale mixing"

study. Anionic polymerization is one of the three most important polymerizations and has an important function in producing thermoplastic rubber [13]. In addition, currently available experimental data on anionic polymerization are limited because of sensitivity to traces of impurities, such as water, alcohol, and oxygen [19, 20]. Therefore, a case study based on the new CFD model was conducted to optimize macroscale parameters and polymer microstructure distributions in a styrene anionic polymerization tubular reactor.

2 Model development

2.1 Polymerization kinetics and method of moments

Styrene anionic polymerization is initiated by sec-butyl lithium and is performed in cyclohexane. Polymerization mechanism is shown as below:

$I + M \xrightarrow{k_i} P_1^{\bullet}$ (1) $P_{n-1}^{\bullet} + M \xrightarrow{k_p} P_n^{\bullet} \quad n = 2,\ 3,...$

(2) $P_n^{\bullet} \xrightarrow{k_t} P_n \quad n = 1, 2, , 3,...$ (3) Where, I , M , $P_n^{\bullet}$, P_n are initiator, monomer, active growing polymer of length *n*, and terminated polymer of length *n*, respectively. k_i , k_p , k_t are initiation rate constant, propagation rate constant, and termination rate constant, respectively. According to reaction mechanisms, relevant reaction kinetic equations are:

$r_I = -k_i[I][M]$ (4) $r_M = -k_i[I][M] - k_p[P_n^{\bullet}][M]$

(5) $r_{P_1^{\bullet}} = k_i[I][M] - k_p[P_1^{\bullet}][M] - k_t[P_1^{\bullet}]$ (6)

$r_{P_n^{\bullet}} = k_p[M]([P_{n-1}^{\bullet}] - [P_n^{\bullet}]) - k_t[P_n^{\bullet}] \quad n \geq 2$ (7) $r_{P_n} = k_t[P_n^{\bullet}] \quad n \geq 1$

(8) In general, polymer chain length n is within the range of 10^3 to 10^5. Apparently, processing various differential equations by CFD is impossible. Based on such consideration, method of moments is introduced to rewrite polymerization kinetic equations [21]. The method of moments is a simple deterministic method widely applicable in modeling various polymerization processes [22]. What's more, the use of the method of moments is for average polymer chain properties, which reflect the behavior of the micro-scale mixing. The m-th moment of active growing polymer, terminated polymer, and polymer are defined respectively as follows [21,23,24]:

$\mu_m = \sum_{n=1}^{\infty} n^m [P_n^{\bullet}]$ (9) $\lambda_m = \sum_{n=1}^{\infty} n^m [P_n]$

(10) $\omega_m = \mu_m + \lambda_m$ (11) By substituting defined moments into polymerization kinetics equations, the moment equations for various species are obtained and shown in Tab. S1 (Supporting Information). Therefore, calculation expressions for M_n, M_w, and PDI are:

$M_n = \frac{\mu_1 + \lambda_1}{\mu_0 + \lambda_0} M_M = \frac{\omega_1}{\omega_0} M_M$ (12) $M_w = \frac{\mu_2 + \lambda_2}{\mu_1 + \lambda_1} M_M = \frac{\omega_2}{\omega_1} M_M$

(13) $PDI = \frac{M_w}{M_n} = \frac{\omega_0 \omega_2}{\omega_1^2}$ (14) 2.2 The CFD model

The CFD model mainly consists of continuity equation, momentum equation, energy equation, material conservation equations and turbulent model (see Eqs. S1-S6 in

Supporting Information). It is assumed that all polymer products are soluble in cyclohexane solvent; therefore, the CFD model can be processed according to single-phase flow. So, the CFD governing transport equations can be written as follows:

Continuity equation

$$\nabla\bullet(\rho\vec{v})=0 \quad (15)$$ Momentum equation

$$\nabla\bullet(\rho\vec{v}\vec{v})=-\nabla p+\nabla\bullet(\bar{\bar{\tau}})+\rho\vec{g}+\vec{F} \quad (16)$$ in which,

$$\bar{\bar{\tau}}=\mu[\nabla\vec{v}+\nabla\vec{v}^{T}]-\frac{2}{3}\nabla\bullet\vec{v}\bar{\bar{I}} \quad (17)$$ Where μ is the viscosity of fluid related to both shear rate and polymer mass fraction for non-Newtonian fluid. The Carreau-Yasuda model is usually used to model non-Newtonian fluid rheology [25,26]. The detailed information for the calculation of μ is given in the Supporting Information (see Eqs. S7 and S8).

Energy conservation equation

$$\nabla\bullet(\vec{v}(\rho e+p))=\nabla\bullet(k_{eff}\nabla T-\sum_{j}h_j\vec{J}_j+(\bar{\bar{\tau}}_{eff}\bullet\vec{v})+S_h \quad (18)$$ where

$$e=\sum_{j}Y_j h_j+\frac{v^2}{2} \quad (19)\ h_j=\int_{T_{ref}}^{T}c_{p,j}dT \quad (20)$$ In Eq. (18), S_h represents polymerization heat given by Eq. (21) based on polymerization kinetics, and only propagation reaction heat was considered in the present study.

$$S_h=r_p\Delta H_r \quad (21)$$ Material conservation equation

$$\nabla\bullet(\rho v W_i)=\nabla\bullet(\rho\overline{D_i}\nabla W_i)+S_i \quad (22)$$ Where W_i, $\overline{D_i}$, S_i are mass fraction, mass diffusivity and reaction source of *i*th species, respectively. The detailed species conservation equations are shown in Tab. S2 (Supporting Information).

3 Simulation conditions and CFD modeling method

3.1 Simulated object and model parameters

The tubular reactor selected from classical literature has 6.35 mm internal diameter, 1.7 m length, and no other structural units. The polymerization system mainly includes sec-butyl lithium initiator, styrene monomer, cyclohexane solvent, and trace amounts of tetrahydrofuran. The simulation assumes that reactants are mixed evenly and subsequently fed into tubular reactor. The parameters used in the model mainly include reactor configuration parameters, operating condition parameters, physicochemical parameters of materials, and setting parameters in the FLUENT software. All parameter values are shown in Tabs. 1 and 2.

3.2 CFD modeling method

In the present study, a commercial CFD code FLUENT 6.3.26 was used to solve these equations described above, and reaction kinetics model was coupled by user-defined function (UDF). All simulations were solved in double mode. A second order upwind method

was employed to discretize all terms in the CFD model. SIMPLE algorithm was used to couple pressure and velocity. Furthermore, 2D meshes were generated by commercial software GAMBIT 2.3.16. To investigate the effect of grid numbers on results, simple grid sensitivity analysis were conducted in advance. When fluid flow regions are meshed by three different quadrangular structured grids, which are composed of 5100, 9600, and 9600 cells in axial direction and 10, 20, and 30 cells in radial direction, respectively; in addition, simulation results of temperature, M_n, and PDI distribution along the tube length are shown in Figs. 1 and 2. Case 1-3 represents three different quadrangular structured grids respectively. It should be noted that the spatial distribution of M_n, and PDI were given only in the reactor inlet section. Apparently, when the grid was greater than 9600×20, temperature, spatial distribution of M_n, and PDI were almost no longer affected by grid number. Considering the computation time and accuracy, a total of 9600×20 cells were selected. Furthermore, all simulations were performed in an Intel Xeon 4 CPU running on 2.83 GHz with 8 GB RAM.

4 Results and discussion

As described above, a new model that couples CFD technology and method of moments, which can predict multi-scale mixing behavior in polymerization tubular reactors, was developed to achieve a triplet "operation condition–macroscale mixing–microscale mixing" study. In this section, three sub-sections were mainly discussed, namely, model verification, effect of polymerization kinetics and effect of some important operating condition parameters on macroscale mixing and microscale mixing under steady state.

4.1 The verification of model

Fig. 3 shows the PDI comparisons of our CFD model, experiment, ideal plug flow model, and classical CFD model at different styrene feed concentrations, where the PDI is calculated from the average value of reactor outlet. Meszéna and Johnson [14] found that the simulation results obtained using the ideal plug flow model are unaffected by the styrene feed concentration. One possible reason behind this finding is that the imperfect mixing is not considered in the ideal plug flow model. Fig. 3 also presents that our CFD simulation results are almost consistent with the experimental results at different feed concentration. Styrene Feed concentration plays a vital role in affecting polymer PDI. In addition, it is obvious that the PDI increases significantly with the increasing of monomer feed concentration. The effect of styrene feed concentration on multi-scale fields will be discussed in more details in Sect. 4.3.2.

In summary, although some assumptions are introduced in our CFD model, our simulation results are basically consistent with classical simulation and experimental results. Therefore, the model can be used to describe styrene anion polymerization system flow fields in tubular reactor.

4.2 The effect of polymerization kinetics model

For anionic polymerization system, the importance of polymerization kinetics is evident. In practice, both chain transfer and chain termination reactions may exist in anionic polymerization system. Specifically, chain transfer reaction to solvent is always highly significant when the reaction temperature is high [13]. However, for anionic polymerization, chain transfer reaction rate is about five orders of magnitude smaller than chain propagation reaction rate; therefore, this parameter is usually negligible [27]. Kim and Nauman [13] had

also studied chain termination reaction of styrene anionic polymerization that was inactivated gradually.

Fig. 4 illustrates the effect of different reaction kinetics on simulation results. In general, polymerization kinetics will affect reaction heat, which directly affects temperature distribution (Fig. 4a) (all contours figures are not drawn to scale; refer to figures below). In this study, temperature distributions are basically identical under two different kinds of polymerization kinetics model. What's more, the chain termination reaction has limited effect on monomer conversion (data are not shown here), which can also be reflected by styrene mass fraction distribution (Fig. 4b). Such limited effect is caused by the chain termination reaction that consumed no styrene monomer. However, chain termination reaction can affect both M_n and PDI. Corresponding contours are shown in Figs. 4c and 4d. When chain termination reaction is considered, M_n decreases from 40904 to 40060, whereas PDI increases from 1.025 to 1.047. Similar simulation results are also reported by Mastan et al. [28], and accumulation of oligomer in the system may be a possible reason for these results. In addition, the dead polymer is mainly generated close to the reactor wall and far from the reactor inlet (see Fig. S1 in Supporting Information). Notably, the average mass fraction of dead polymer in tubular reactor outlet is only 0.119 %, which can be ignored. The abovementioned discussion indicates that chain termination reaction has limited effect on simulation results for our anionic polymerization system. If not specified otherwise, ideal anionic polymerization kinetic model is selected in the following simulations for computational cost.

4.3 The effect of operating conditions

4.3.1. Flow velocity

Figs. 5 and 6 show the influence of flow velocity on flow fields, in which styrene and sec-butyl lithium feed concentration is 0.47 mol/L and 0.001 mol/L, respectively, and the selected flow velocities are 0.0265, 0.0530, 0.0795, and 0.1060 m/s.

Fig. 5a illustrates that flow velocity will affect monomer conversion distribution in the tubular reactor inlet. When flow velocity is 0.0265 m/s, polymerization is performed adequately at the tubular reactor inlet where styrene conversion reaches almost 100%; this process may result in easier initiation of reactor overheating. With increased flow velocity, monomer conversion receives a significant decline because of the low residence time. Fig. 5b shows the effect of flow velocity on temperature distribution. It is obvious that temperature rises first and then gradually decreased along with the tubular reactor. As described above, polymerization is performed intensively at the reactor inlet where the highest temperature turns up. One knows that a higher velocity will make styrene distribution more even, therefore, polymerization reaction proceeds uniformly. What's more, convective heat transfer rate increases with increasing flow velocity. In this study, however, the reactor temperature increases with the increasing of flow velocity. It means that reaction heat is the main factor influencing the temperature distribution in tubular reactor. The influence of flow velocity on M_n is shown in Fig. 6a. We have known that flow velocity will affect the temperature and polymerization rate, which in turn results in molecular property distributions. When flow velocity increases from 0.0265 to 0.106 m/s, the M_n at the reactor outlet varies from 22472 to 42950 g/mol according to our CFD simulation results. Fig. 6b illustrates the effect of flow velocity on PDI. When the simulation is performed under the

different flow velocity, although PDI exhibits a big difference at the reactor inlet, the flow velocity has little impact on PDI at the reactor outlet. As we all known, M_n and PDI are mainly determined by polymerization kinetics; however, these parameters will also be affected by mass and heat transfer. Yadav et al. [29] also found that better temperature control on tubular reactors can lead to narrower molecular weight distribution of polymer product. In terms of chemical process, increase in flow velocity also means an increase in energy consumption; therefore, economic costs, production capacity, and product properties must be considered when selecting an appropriate flow velocity.

4.3.2. Styrene feed concentration

Figs. 7 and 8 describe the effect of styrene feed concentration on monomer conversion, temperature and M_n. Fig. 7 shows that feed concentration plays a vital role in affecting styrene conversion distribution. Anionic polymerization is extremely fast that this value differs from other types of polymerization. Styrene conversion reaches 95% soon after styrene reaches the reactor. In the current paper, with the feed concentration increased, monomer conversion increases rapidly, resulting that polymerization mainly occurs in the reactor inlet; therefore, the tubular reactor comprises two zones, namely, polymerization control zone and transfer control zone. Moreover, both zones can affect polymer microscopic structure. From the Fig. 8a, similar temperature prediction results are observed here when compared with the simulation results under different flow velocity. It shows that when feed concentration is low, temperature distribution is relatively uniform within the reactor; however, when styrene feed concentration increases to 0.94 mol/L, the reactor overheating phenomenon becomes extremely apparent, and the highest temperature reaches 329 K. Certainly, the main reason is the poor mixing in tubular reactor. Zhang et al. [30] revealed that imperfect mixing of reactants might create entirely different polymerization rates, which leads to local hot spots that can initiate polymer decomposition. Similar research was also conducted by Kolhapure and Fox [9], who provided some important information to avoid reactor thermal runaway. Fig. 8b clearly shows that M_n distribution is strongly dependent on styrene feed concentration. Higher styrene feed concentration leads to greater M_n value. Furthermore, some interesting similarities on M_n distribution and temperature are found in tubular reactor. When feed concentration is low, both temperature and M_n distribution are uniform. When styrene feed concentration is increased, however, a large number of high polymers are generated in the overheating region, and the degree of reactor overheating directly affects M_n distribution.

5 Conclusions

In the current study, we have developed a CFD model to simulate styrene anionic polymerization system flow fields in tubular reactor. In addition, quantitative relationships among operating conditions, macrocosmic flow fields, and microcosmic flow fields were developed by coupled CFD model with moment equations. The effects of different polymerization kinetics models on flow fields were studied and found that chain termination reaction had limited effect on simulation results for styrene anionic polymerization system. Furthermore, effect of reactor operating conditions on macroscopic flow fields based on the model, as well as the mechanisms that lead to the influence of macroscopic flow fields on microscopic flow fields through polymerization reaction, mass and heat transfer were also studied. Flow velocity and styrene feed concentration play an important role in affecting

monomer conversion, temperature, M_n and PDI distributions. Reaction heat is the main factor influencing the temperature distribution in tubular reactor, while M_n and PDI are mainly determined by polymerization kinetics that will also be affected by mass and heat transfer. In summary, the current paper originally described quantitative relationships among reactor operating conditions, macroscopic flow fields, and microscopic flow fields. This study offered a new way of optimizing reactor operation conditions and preparing single dispersion polymer products.

Acknowledgments

The authors thank the National Ministry of Science and Technology of China (No. 2012CB21500402), the National Natural Science Foundation of China (No. U1462101) and the Research Fund for the Doctoral Program of Higher Education (No. 20130073110077) for supporting this work.

Symbols used

$C_{p,j}$	[$m^2 s^{-2} K^{-1}$]	specific heat of species j
D	[m]	tube diameter
D_I	[$m^{-2} s^{-1}$]	initiator diffusion coefficient
D_M	[$m^{-2} s^{-1}$]	monomer diffusion coefficient
$\overline{D}$	[$m^{-2} s^{-1}$]	average diffusion coefficient of polymer chain
e	[$m^2 s^{-2}$]	total energy
F	[kg $m^{-2} s^{-1}$]	external forces
g	[m s^{-2}]	gravitational acceleration
h	[W $m^{-2} K^{-1}$]	heat transfer coefficient
h_0	[$m^2 s^{-2}$]	static enthalpy
h_j	[$m^2 s^{-2}$]	enthalpy of species j
ΔH_r	[J mol^{-1}]	reaction enthalpy
I	[-]	initiator
$\overline{I}$	[-]	unit tensor
J_j	[kg $m^{-2}s^{-1}$]	diffusion flux of species j
k_{eff}	[W $m^{-1}K^{-1}$]	effective conductivity
k_i	[m^{-3} $mol^{-1}s^{-1}$]	initiation rate constant
k_p	[m^{-3} $mol^{-1}s^{-1}$]	propagation rate constant
k_t	[m^{-3} $mol^{-1}s^{-1}$]	termination rate constant
L	[m]	tube length
M	[-]	styrene monomer
M_n	[kg mol^{-1}]	number average molecular weight
M_M	[kg mol^{-1}]	monomer molecular weight
M_w	[kg mol^{-1}]	weight average molecular weight
p	[Pa]	pressure
P_n	[-]	terminated polymer of length *n*
$P_n^{\bullet}$	[-]	active growing polymer of length n
r_i	[mol m^{-3} s^{-1}]	rate of initiation

r_p	[mol m^{-3} s^{-1}]	rate of propagation
r_t	[mol m^{-3} s^{-1}]	rate of termination
S_h	[W m^{-3}]	source term in energy equation
t	[s]	time
T	[K]	temperature
T_{ref}	[K]	the reference temperature
v	[m s^{-1}]	velocity
W_i	[-]	the mass fraction of species *i*

Greek symbols

ρ	[kg m^{-3}]	density
μ	[Pa s]	dynamic viscosity
μ_m	[-]	the m-th moment of activate growing polymer
λ	[W m^{-1} K^{-1}]	thermal conductivity of reaction mixture
λ_m	[-]	the m-th moment of terminated polymer
ω_m	[-]	the m-th moment of polymer
τ	[Pa]	stress tensor

References

[1] N. Agrawal, G. P. Rangaiah, A. K. Ray, S. K. Gupta, *Chem. Eng. Sci.* 2007, *62*, 2346-2365.

[2] N. Chan, M. F. Cunningham, R. A. Hutchinson, *Polym. Chem*. 2012, *3*, 1322-1333.

[3] C. C. Chen, E. B. Nauman, *Chem. Eng. Sci.* 1989, *44*, 179-188.

[4] S. Fan, S. P. Gretton-Watson, J. H. G. Steinke, E. Alpay, *Chem. Eng. Sci.* 2003, *58*, 2479-2490.

[5] S. Lynn, J. E. Huff, *AIChE J.* 1971, *17,* 475–481.

[6] H. Mavridis, C. Kiparissides, *Process Eng.* 1985, *3*, 263-290.

[7] R. Tomovska, J. C. de la Cal, J. M. Asua, *Ind. Eng. Chem. Res.* 2014, *53*, 7313-7320.

[8] N. Jongen, M. Donnet, P. Bowen, J. Lemaître, H. Hofmann, R. Schenk, C. Hofmann, M. Aoun-Habbache, S. Guillement-Fritsch, J. Sarrias, A. Rousset, M. Viviani, M. T. Buscaglia, V. Buscaglia, P. Nanni, A. Testino, J. M. Herguijuela, *Chem. Eng. Technol.* 2003, *26*, 303-305.

[9] N. H. Kolhapure, R. O. Fox, *Chem. Eng. Sci.* 1999, *54*, 3233-3242.

[10] S. F. Roudsari, F. Ein-Mozaffari, R. Dhib, *Chem. Eng. J.* 2013, *219*, 429-442.

[11] Y. P. Zhu, G. Q. Chen, Z. H. Luo, *Macromol. React. Eng.* 2014, *8*, 609-621.

[12] Y. P. Zhu, Z. H. Luo, J. Xiao, *Comput. Chem. Eng.* 2014, *71*, 39-51.

[13] D. M. Kim, E. B. Nauman, *Ind. Eng. Chem. Res.* 1999, *38*, 1856-1862.

[14] Z. G. Meszéna, A. F. Johnson, *Macromol. Theory Simul.* 2001, *10*, 123-135.

[15] X. Inglès, J. Pallares, M. T. Larre, L. Méndez, F. X. Grau, *J. Ind. Eng. Chem.* 2013, *19*, 1251–1256.

[16] W. Zhou, E. Marshall, L. Oshinowo, *Ind. Eng. Chem. Res.* 2001, *40*, 5533-5542.

[17] R. O. Fox, *Rev.LInst. Fr. Pet.* 1996, *51*, 215-243.

[18] R. O. Fox, *Chem. Eng. Process.* 1998, *37*, 521-535.

[19] K. Iida, T. Q. Chastek, K. L. Beers, K. A. Cavicchi, J. Chun, M. J. Fasolka, *Lab Chip.* 2009, *9*, 339-345.

[20] S. A. Murphy, Z. G. Meszéna, A. F. Johnson, *Polym. React. Eng.* 2001, *9*, 227-247.

[21] S. Zhu, *Macromol Theory Simul.* 1999, *8*, 29−37.

[22] E. Mastan, S. Zhu, *Eur. Polym. J.* 2015, *68*, 139-160.

[23] R. Wang , Y. W. Luo, B. G. Li, X. Y. Sun, S. Zhu, *Macromol. Theor. Simul.* 2006, *15*, 356–368.

[24] S. Zhu, *J. Polym. Sci. Pol. Phys.* 1999, *37*, 2692-2704.

[25] J. Pohn, M. Cunningham, T. F. L. Mckenna, *Macromol. React. Eng.* 2013, *7*, 380-392.

[26] M. Pishvaei, C. Graillat, T. F. McKenna, P. Cassagnau, *J. Rheol.* 2007, *51*, 51-69

[27] A. L. Gatzke, *J. Polym. Sci., Part A: Polym. Chem.* 1969, *7*, 2281-2292.

[28] E. Mastan, D. P. Zhou, S. Zhu, *Macromol. Theory Simul.* 2014, *23*, 227-240.

[29] A. K. Yadav, M. J. Barandiaran, J. C. de la Cal, *Macromol. React. Eng.* 2014, *8*, 467-475.

[30] S. X. Zhang, N. K. Read, W. H. Ray, *AIChE J.* 1996, *42*, 2911-2925.

Tables

Table 1. Physical property of species at 20°C and 1atm [14].

Species	Density [kg m^{-3}]	Diffusion coefficient [m^2 s^{-1}]	Viscosity [Pa s]	M_w [kg $kmol^{-1}$]
Styrene	909	$1 \cdot 10^{-9}$	$7.49 \cdot 10^{-4}$	104
sec-butyl lithium	680	$1 \cdot 10^{-9}$	0.034	63
polymer	1 000	0	-	10^2～10^5

Table 2. Model parameters [14].

Descriptions	Values
Physicochemical parameters of fluid	
ρ [kg m^{-3}]	880
C_p [J kg^{-1} K^{-1}]	1700
λ [W m^{-1} K^{-1}]	0.2
h [W m^{-2} K^{-1}]	100
ΔH_r [J mol^{-1}]	60000
Operating conditions parameters	
Feed flow rate [ml min^{-1}]	50～200
Styrene feed concentration [mol L^{-1}]	0.0147～1.30
Initiator feed concentration [mol L^{-1}]	0.001
Feed temperature [K]	293.15
Settings parameters in the software	
Operating pressure [Pa]	100000
Inlet boundary condition	Velocity inlet
Outlet boundary condition	Pressure outlet
Wall boundary condition	No slip for fluid
Wall temperature [K]	293.15
Convergence criteria	$1 \cdot 10^{-5}$

Figures

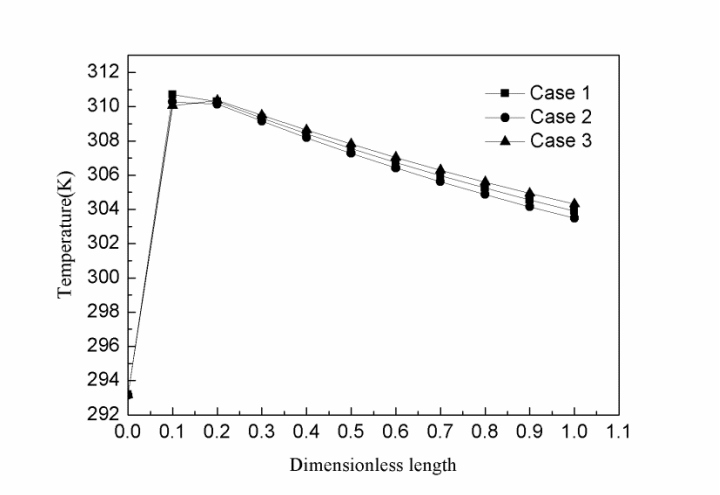

Figure 1. Grid sensitivity analysis: the contours of temperature under steady state.

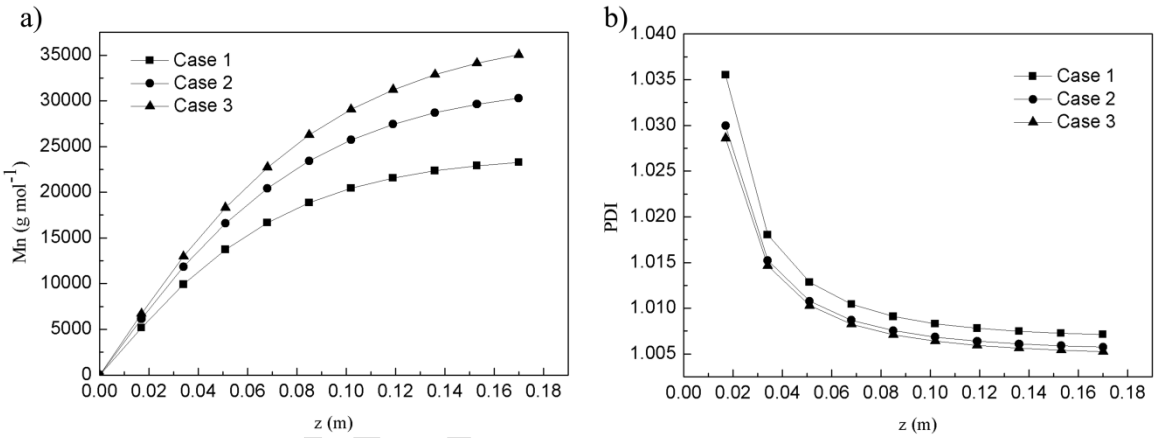

Figure 2. Grid sensitivity analysis: the contours of M_n and PDI under steady state.

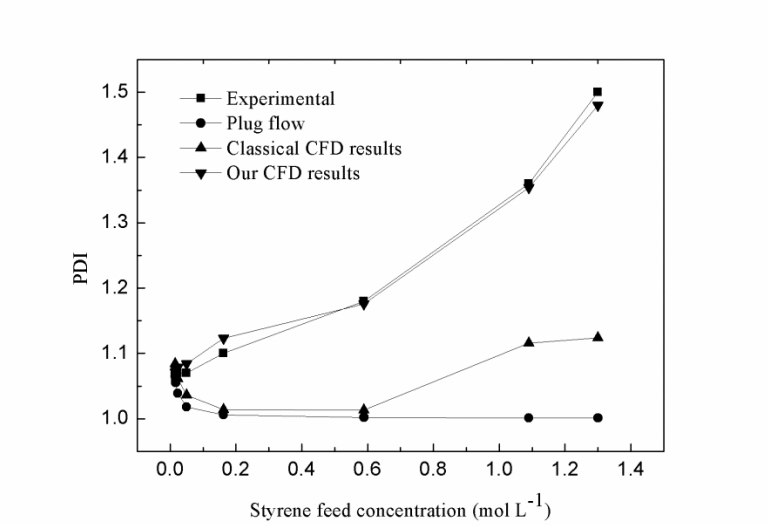

Figure 3. Comparison of our CFD simulation results with the classical data [14].

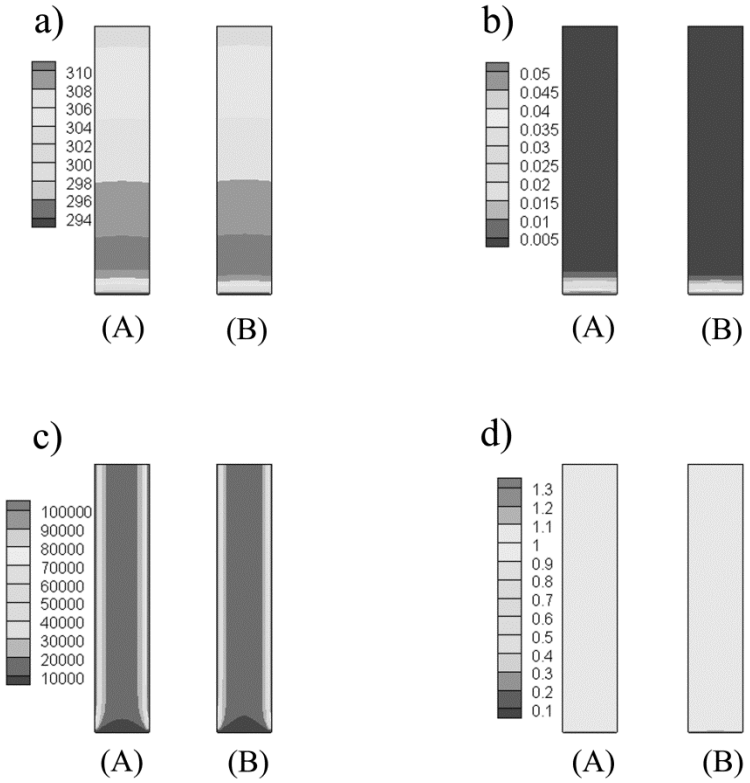

Figure 4. The contours of a) temperature, b) styrene concentration, c) M_n, d) PDI under steady state: (A) no termination, (B) have termination.

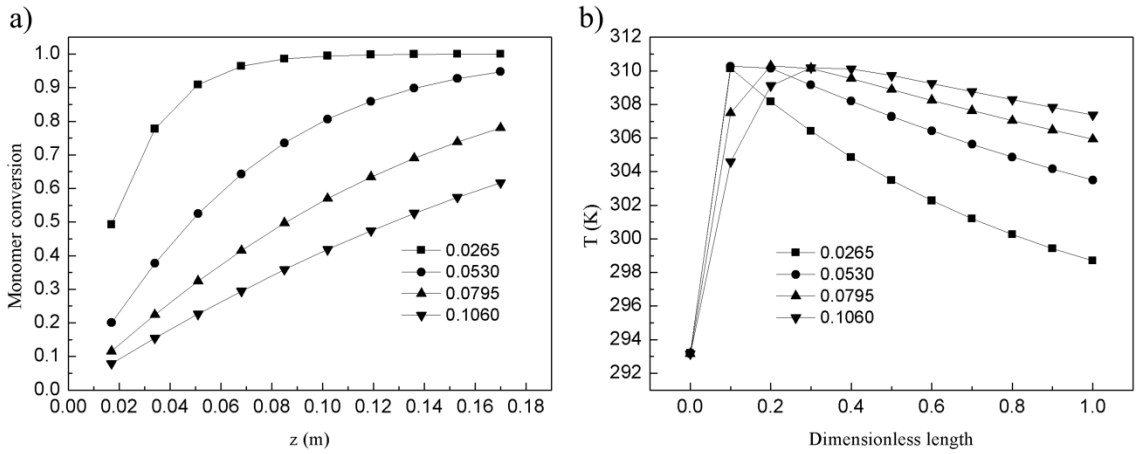

Figure 5. The influence of velocity on styrene conversion and temperature.

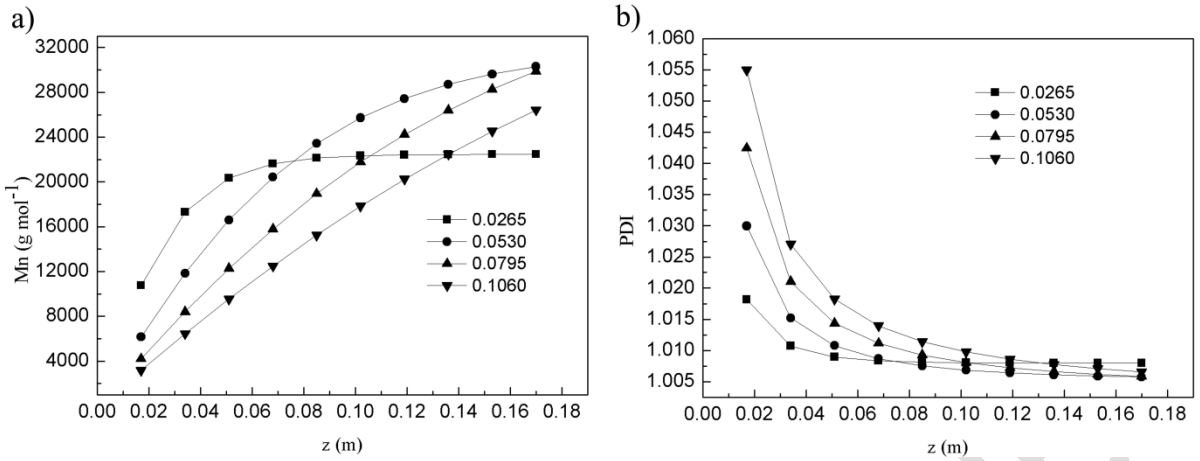

Figure 6. The influence of velocity on M_n and PDI.

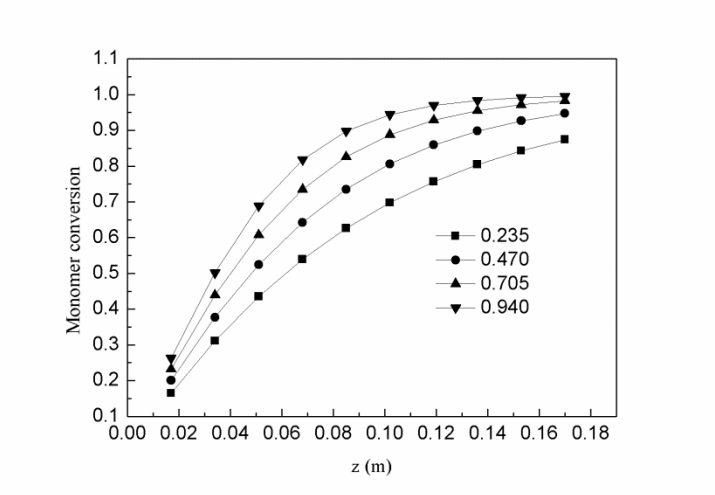

Figure 7. The influence of styrene feed concentration on conversion.

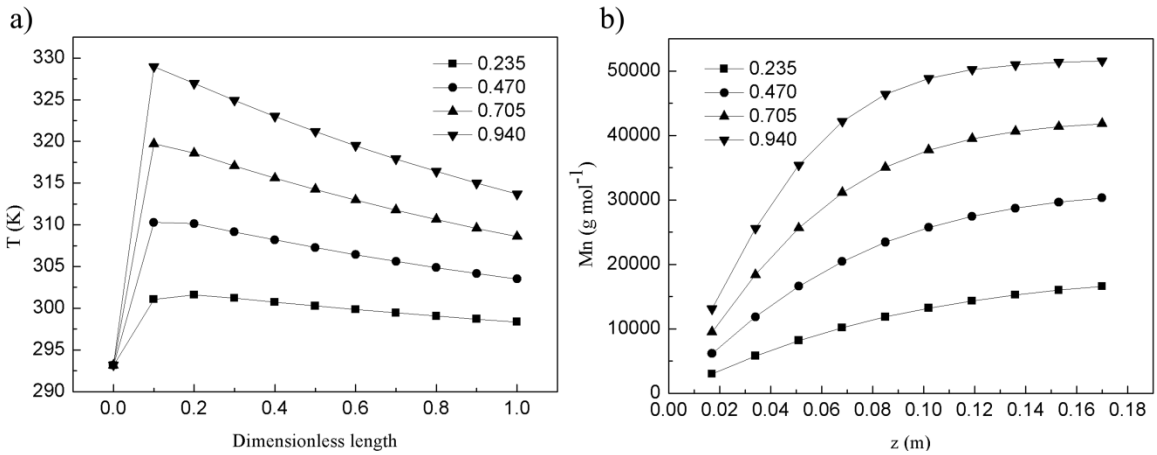

Figure 8. The influence of styrene feed concentration on temperature and M_n.

Table of Contents

Coupling of CFD technology and method of moments to form a uniquely coupled model was used to describe multi-scale mixing field in a styrene anionic solution polymerization tubular reactor. The triplet “operation condition–macroscopic-scale mixing–microscopic-scale mixing” study was pointed out based on the coupled model.

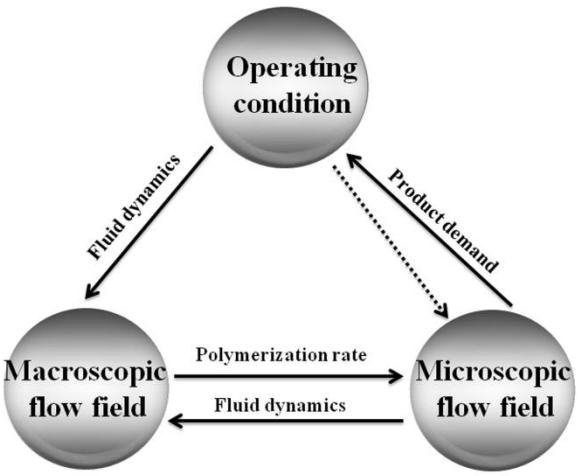

The relationships among operating condition, macroscopic flow field and microcosmic flow field.